PHYSICAL REVIEW D VOLUME 18, NUMBER 1 1 JULY 1978

Partial-wave analysis of the $\bar{K}N$ system from 360 to 1320 MeV/c

M. Alston-Garnjost, R. W. Kenney, D. L. Pollard, R. R. Ross, and R. D. Tripp
Lawrence Berkeley Laboratory, University of California, Berkeley, California 94720

H. Nicholson
Mt. Holyoke College, South Hadley, Massachusetts 01075

M. Ferro-Luzzi
CERN, 1211 Geneva 23, Switzerland

(Received 16 January 1978)

In this paper we use new data from several recent $\bar{K}N$ experiments in conjunction with older data to make an energy-dependent partial-wave analysis of the $\bar{K}N$ system. The important new additions never used before in a partial-wave analysis are our precision measurements of the charge-exchange total cross sections, our measurements of the charge-exchange angular distributions, and the first measurements of the K^-p polarization at these low momenta. A new feature introduced in the analysis is the S-wave cusp treatment at the $\Lambda\eta$ and $\Sigma^0\eta$ thresholds, which we find necessary to describe the observed behavior in the charge-exchange total cross sections near these thresholds. Other features include a single-channel unitary formulation for resonances and backgrounds and a parametrization of these amplitudes incorporating centrifugal-barrier effects. New values for masses, widths, and elasticities for resonances in this region are reported and better evidence is found for several of the less well established resonances. None of the new resonances suggested by recent $I = 0$ and $I = 1$ total-cross-section measurements are required. Fits are displayed for all the data used and predictions of this partial-wave analysis are compared with those of two other recent analyses for certain quantities yet to be measured. A table of the amplitudes, in steps of 20 MeV/c, is provided.

I. INTRODUCTION

During the past several years, a number of experiments have been done with counters and with bubble chambers which have considerably improved the precision of measurements in the $\bar{K}N$ system. For this reason we have undertaken a new partial-wave analysis of the $\bar{K}N$ channel in order to search for new structures and to re-evaluate the resonances derived from analyses of the older experiments.

We have chosen to study the $\bar{K}N$ channel alone rather than perform a multichannel analysis since most of the new data are from the elastic and charge-exchange reactions. The other two-body channels ($\Lambda\pi$, $\Sigma\pi$, $\Lambda\eta$, $\Sigma\eta$) are exceedingly useful when the resonances have dominant branching fractions into these channels, hence a low elasticity. However, essentially all the information on resonant structure in these reactions can be obtained via single-channel analyses, because at the energies under consideration most of the beneficial constraints of a multichannel analysis are lost due to the complicating presence of several additional three- and four-body channels with substantial cross sections. Only at low energies where the three-body cross sections become small has a multichannel analysis been found to be really useful.[1]

The momentum spanned by this analysis, 360 to 1320 MeV/c ($1507 < E_{c.m.} < 1941$ MeV), was dictated by the available new data and by the existence of prominent resonances with well-established quantum numbers, at the lower and upper energies, with which to anchor the analysis. Experience has shown that an energy-dependent partial-wave analysis in regions with such resonances leads to an unambiguous determination of the various amplitudes. In energy regions devoid of prominent resonances the amplitudes become much less certain. The latter is the case for the $\bar{K}N$ system from above 400 MeV/c to at least 700 MeV/c. Thus we found it essential to extend our analysis downward in momentum to 360 MeV/c in order to encompass the prominent $\Lambda(1520)$ resonance and thereby stabilize the other partial-wave amplitudes whose behaviors are uncertain. For this we also benefited from the recently published high-statistics bubble-chamber coverage of the $\Lambda(1520)$ region.[2] The upper limit was likewise determined by the coexistence of the very elastic $\Lambda(1815)$ resonance and the new high-statistics bubble-chamber experiment of the Rutherford Laboratory and Imperial College (RL-IC).[3]

Among the numerous $\bar{K}N$ partial-wave analyses[4-10] there has been general agreement concerning resonances in the higher-angular-mo-

mentum states. Only among the S- and P-wave amplitudes, where the nonresonant background is usually very large, have significantly different conclusions been drawn from the data. Often these differences are clearly apparent from inspection of the Argand diagrams. In other cases the Argand diagrams are similar, and much of the difference in the resonances can be ascribed to differences in the parametrization of backgrounds and in the way in which resonances are combined with backgrounds.

In this paper we describe in detail a partial-wave analysis reported earlier.[9] We also present the results from a new fit with an expanded data bank containing our recently measured charge-exchange angular distributions[11] and having, in addition, constraints on the K^-p and Kn forward scattering amplitudes derived from a new dispersion-relation calculation.[12]

II. DATA

Table I shows the various types of data used, their sources, and their contributions to χ^2 in the best fit we obtained. Of the many bubble-chamber experiments in this region, we have included only those designed to study in a systematic way the energy dependence of structures arising from the formation of resonances. Thus we have left out a number of older experiments of low precision or of limited momentum coverage, but rely heavily, as do most previous analyses, on the extensive data of the CERN-Heidelberg-Saclay (CHS) collaboration.[13] As discussed in the introduction, new accurate bubble-chamber data[2,8,14] have also contributed substantially to this analysis. Recent bubble-chamber results[15] for the reaction $K_L p \to K_S p$ have not been included since they involve assumptions concerning the positive-strangeness KN interaction, thus introducing additional and unknown systematic uncertainties. Nor were the very sparse data currently available on K^-n elastic scattering from two older bubble-chamber experiments[16] considered to be of sufficient statistical weight to be included.

For reasons of economy the computer program was limited to 100 discrete momenta. Since the various experiments were done at many more momenta, it was necessary to interpolate some of the data points; in the case of experiments of low statistical accuracy we simply displaced the published momentum, typically by a few MeV/c.

A. K^-p elastic scattering

The bulk of the K^-p differential cross section data comes from bubble chambers, with improved statistical accuracy from a recent Birmingham-Rutherford electronic experiment[17] over the central third of our momentum region. Instead of fitting the differential cross sections directly we have, for economy of computation, fitted both the shape-dependent ratios A_n/A_0 of the Legendre-polynomial coefficients through $n=6$ and the integrated cross section ($\sigma = 4\pi\lambda^2 A_0$). Correlations between the various orders of polynomial coefficients have not been included. The uncertainty

TABLE I. Data used in the fit.

Type of data	References	Momentum (MeV/c)	Data points	χ^2
(1) $d\sigma/d\Omega(K^-p)$	2	365– 425	35	113
	13	436–1200		
	3	960–1320	396	360
	17	610– 943		
(2) $d\sigma/d\Omega(180°, K^-p)$	2,3,13,21	365–1320	51	113
(3) $D(K^-p), D(K^-n)$	12	375–1320	22	63
(4) K^-p polarization	23	650–1071	135	229
	22	865–1330	374	389
(5) $d\sigma/d\Omega(\bar{K}^0 n)$	2	365– 425	35	93
	13	436–1200		
	14	862–1011	295	483
	3	960–1320		
	11	515– 956	132	312
(6) $\sigma(\bar{K}^0 n)$	24	515–1066	48	113
(7) σ_T	2	365– 425	7	28
	27	436–1066	36	55
	25,28	1080–1320	7	22
(8) σ_0, σ_1	27	436–1066	72	129
	25,28	1080–1320	14	21
Total			1659	2523

on the integrated cross section depends mostly on the accuracy of the K^- flux determination; hence it is essentially independent of the measurement of the shape. We have also explicitly fitted the K^-p differential cross section at 180°. Most of the points were obtained by extrapolation of bubble-chamber data, there having been but one ad-hoc counter experiment[21] to measure this quantity. Although this was a redundant use of the data described by the polynomial coefficients, it served to better constrain the fit in the backward direction which, for certain momenta, was particularly difficult to fit.

Only a few measurements[18] of the K^-p and K^-n forward scattering amplitudes have been made in the resonance region. However, they can be calculated with some reliability at all energies by means of a dispersion relation using all the available $K^\pm N$ forward scattering measurements and the total cross sections. For this we have used a new dispersion-relation determination of the real parts of the K^-p and K^-n forward scattering amplitudes[12] which incorporates all of the very low energy K^-p data, the recently measured real parts at higher energies,[18] and, in contrast to previous determinations,[19] is constrained to yield the observed dip in the charge-exchange differential cross section at 300 MeV/c.[2,20] These results have been used in our partial-wave analysis by introducing as data points the real parts of the K^-p and K^-n forward scattering amplitudes at approximately 100 MeV/c intervals with uncertainties of ±0.05 F.

Polarization in K^-p elastic scattering has previously been measured only above 860 MeV/c.[22] This has now been extended down to 650 MeV/c by recent measurements at BNL.[23] The polarization has been fitted directly at all angles and energies for which it has been measured. This was preferable to fitting the polarization coefficients because these coefficients involve an expansion of the product of the differential cross section times the polarization, and therefore contain two independent measurements.

B. Charge-exchange scattering

For this reaction, polarization measurements have not yet been made; only the angular distributions and total cross sections have been measured. We again fit the shape-dependent angular distribution coefficients A_n/A_0 and the total charge-exchange cross section. Our precision measurements[24] of the latter dominate the much less accurate bubble-chamber data over most of the momentum region covered by the analysis, while our recent measurements of the angular distributions for charge-exchange scattering[10] are also of substantially higher statistical accuracy than the bubble-chamber data.

C. Total cross sections

The other precision data used in this analysis are the total K^-p cross sections. Below 1 GeV/c these have been measured by three counter experiments.[25-27] We have preferentially used the most recent and accurate measurements of BNL,[27] interpolated to momenta where other types of data exist. Between 360 and 430 MeV/c we have relied on bubble-chamber measurements[12] of these cross sections, while above 1 GeV/c other counter experiments were used.[25,28]

The individual $I=0$ and $I=1$ total cross sections were also fitted. Below 1 GeV/c these were obtained from the analysis of Carroll *et al.*[27] Because there is considerable disagreement between the various determinations of the isospin-decomposed cross sections, and because of the uncertainties associated with the deuterium corrections, we have enlarged the errors on these derived cross sections to approximately ±5%. A partial-wave analysis of bubble-chamber data in the vicinity of 400 MeV/c[20] suggests an $I=1$ total cross section some 10 mb larger than that of Carroll *et al.* Due to this discrepancy we have restricted the isospin-decomposed cross sections to those above 430 MeV/c.

III. METHOD OF ANALYSIS

The basic partial-wave analysis program is an outgrowth of that used by CHS[4] into which we have incorporated a number of sophistications deemed necessary for the elastic amplitudes in this energy region. Each partial-wave amplitude through $J=\frac{7}{2}$ was given an energy-dependent parametrization, consisting of a nonresonant background upon which, if there were indications of resonant structure in that partial wave, could be superposed one or two Breit-Wigner resonances. An approximation to single-channel unitarity was realized in the conventional way by writing the scattering amplitude T as $T=T_B+S_BT_R$,[29] where the subscripts B and R refer to the background and resonant amplitudes. Two resonances in the same partial wave were similarly combined.

Each background amplitude was made explicitly unitary by parametrizing it in terms of a variable scattering length A, viz.,

$$T_B=\beta A/(1-i\beta A). \tag{1}$$

It is essential to introduce a centrifugal-barrier factor β to accomodate the large momentum in-

terval spanned by the analysis; for this we write[30]

$$\beta = \frac{k}{E}\left(\frac{k^2}{k^2+R^{-2}}\right)^l, \tag{2}$$

where k is the incident c.m. wave number, E is the c.m. energy, R is the radius of interaction, and l is the orbital angular momentum. The complex scattering length is conveniently written as $A = a + ib^2$, so that the imaginary part which represents absorption always remains positive. Further momentum dependence is contained in the coefficients a and b, which are expanded in Legendre polynomials:

$$a = \sum_n a_n p_n(y) \text{ and } b = \sum_n b_n p_n(y). \tag{3}$$

The argument y of the Legendre polynomial $P(y)$ is linearly related to the momentum spanning the fitted interval, $-1 \leq y \leq 1$. For the large S- and P-wave background amplitudes, three complex coefficients were usually found to be necessary in order to achieve a reasonable fit to the data; for the D_3 waves one complex amplitude was sufficient, this being further reduced to one real amplitude for higher waves. Thus D and higher angular momenta backgrounds were parametrized by constant scattering lengths, whereas S- and P-wave backgrounds assumed a more flexible behavior while retaining the unitary feature.

Resonant amplitudes were expressed as Breit-Wigner resonances,

$$T_R = \frac{\Gamma_e}{2(M-E) - i\Gamma}, \tag{4}$$

where E is the c.m. energy. M, the resonance mass, is a free parameter, as are the total width at resonance Γ_r and the elasticity x, related to the elastic width Γ_e and the total width Γ by $x = \Gamma_e/\Gamma$. The energy-dependent widths appearing in Eq. (4), $\Gamma = \beta\Gamma_r/\beta_r$ and $\Gamma_e = \beta\Gamma_{er}/\beta_r$, contain the centrifugal-barrier factor β described previously, with β_r evaluated at resonance. For S_{01}, S_{11}, and P_{01} resonances (we use the conventional notation L_{I2J}) where large nonresonant backgrounds are present, it was found necessary to introduce a phase factor in order to achieve a good fit. In principle, the introduction of this phase factor could result in the combined amplitude exceeding the unitary limit, but in practice these amplitudes always fell within the unitary circle. For several of the prominent resonances, additional parameters allowing for a linear dependence of the elasticity x on the c.m. energy were introduced. Since no significant improvement in the fit was attained by this additional freedom, the elasticities were taken to be independent of energy.

At the thresholds for the processes $K^-p \to \Lambda\eta$ and $K^-p \to \Sigma^0\eta$, a rapid rise has been observed in the reaction cross sections with a subsequent falloff at higher energy, the overall behavior being consistent with S_{01} and S_{11} resonant excitation.[31,32] Accordingly, we have introduced cusps into the elastic parametrization at the thresholds to reflect the observed enhancements in these channels. This was done by adding a partial width for these processes to the total width. Thus,

$$\Gamma_T = \Gamma + \gamma_Y p \tag{5}$$

replaced Γ in the above resonance expressions. Here p is the momentum of the η in the c.m., and Γ is the total width without the η channel, while γ_Λ and γ_Σ are free parameters controlling the strength of the cusp. Since p becomes $+i|p|$ when analytically extended below threshold, the amplitude has a singularity in speed at threshold accompanied by a 90° left-hand turn in the trajectory on an Argand plot as the threshold is traversed from below.[33]

The well-established three- and four-star resonances[34] were introduced from the outset with their accepted values of masses, widths, and elasticities. A minimum was achieved in these conditions by first varying the background parameters and then the parameters of the resonances. Attempts were then made to improve this minimum-structure solution by adding resonances

TABLE II. Resonance parameters. Quantities in brackets are held constant.

State[a] L_{I2J}	M (MeV)	Γ (MeV)	Amplitude[b]
S_{01}****	1671 ± 3	29 ± 5	0.17 ± 0.03
S_{01}**(*)	1725 ± 20	185 ± 20	0.28 ± 0.05
S_{11}***(*)	1770 ± 10	161 ± 20	0.33 ± 0.05
P_{01}*(*)	1703 ± 100	593 ± 200	0.14 ± 0.05
P_{11}**(*)	1679 ± 10	38 ± 10	0.10 ± 0.05
P_{03}***(*)	1908 ± 10	119 ± 20	0.34 ± 0.05
P_{13}****	[1385]	20 ± 10	0.15 ± 0.05
D_{03}****	1520 ± 0.5	15.4 ± 0.5	0.45 ± 0.03
D_{03}****	1692 ± 5	64 ± 10	0.22 ± 0.03
D_{13}****	1679 ± 10	56 ± 20	0.11 ± 0.03
D_{05}****	[1825]	[90]	0.02 ± 0.02
D_{15}****	1777 ± 5	116 ± 10	0.37 ± 0.03
F_{05}****	1819 ± 2	72 ± 5	0.60 ± 0.03
F_{15}****	1937 ± 20	161 ± 20	0.14 ± 0.05
F_{17}****	[2030]	[180]	[0.2]
G_{07}****	[2100]	[250]	[0.3]

[a] Stars show the status of the resonance in 1976 as assigned by the Particle Data Group. Stars in parentheses indicate the changes in this attribution which we believe should be made on the basis of this analysis.

[b] The amplitudes listed correspond to the diameter of the resonant circles. When absorptive processes are present they become $\eta_B\Gamma_e/\Gamma$, where η_B is the absorption parameter of the background.

to those background amplitudes whose energy dependences were suggestive of resonances, or to those partial waves where resonances have previously been identified in the reaction channels $K^-p \to \Sigma\pi$ or $K^-p \to \Lambda\pi$. If a significant improvement in the fit was thereby achieved, the resonance was retained. Several well-established resonances with masses above our fitted region but whose influence was felt at lower energy were introduced with fixed parameters, as was the D_{05} resonance seen clearly only in the $\Sigma\pi$ channel. The best fit has a χ^2 of 2523 with 1659 data points.

IV. RESULTS AND COMPARISON WITH OTHER ANALYSES

The results of this analysis appear in the following tables and figures. Table II lists the resonance parameters obtained in the best fit, while Table III contains those of the background and other parameters. The resulting partial-wave amplitude are tabulated every 20 MeV/c in Table IV. The Argand diagrams for the S and P wave amplitudes are displayed in Fig. 1, where they are compared with those of the RL-IC analysis.[8] In Fig. 2 we exhibit the fits to the total elastic and charge-exchange cross sections, and in Fig. 3 the fits to the polynomial coefficient ratios A_n/A_0 of both angular distributions. Figure 4 shows the fit to the elastic 180° cross section. Fits to the polarization are shown at selected momenta in Fig. 5, where they are compared with two other analyses. The resulting momemtum dependence of the polarization coefficients B_n can be seen in Fig. 6. The total K^-p and individual isospin-decomposed cross sections are shown in Fig. 7, while our real parts of the forward scattering amplitudes for K^-p and K^-n appear

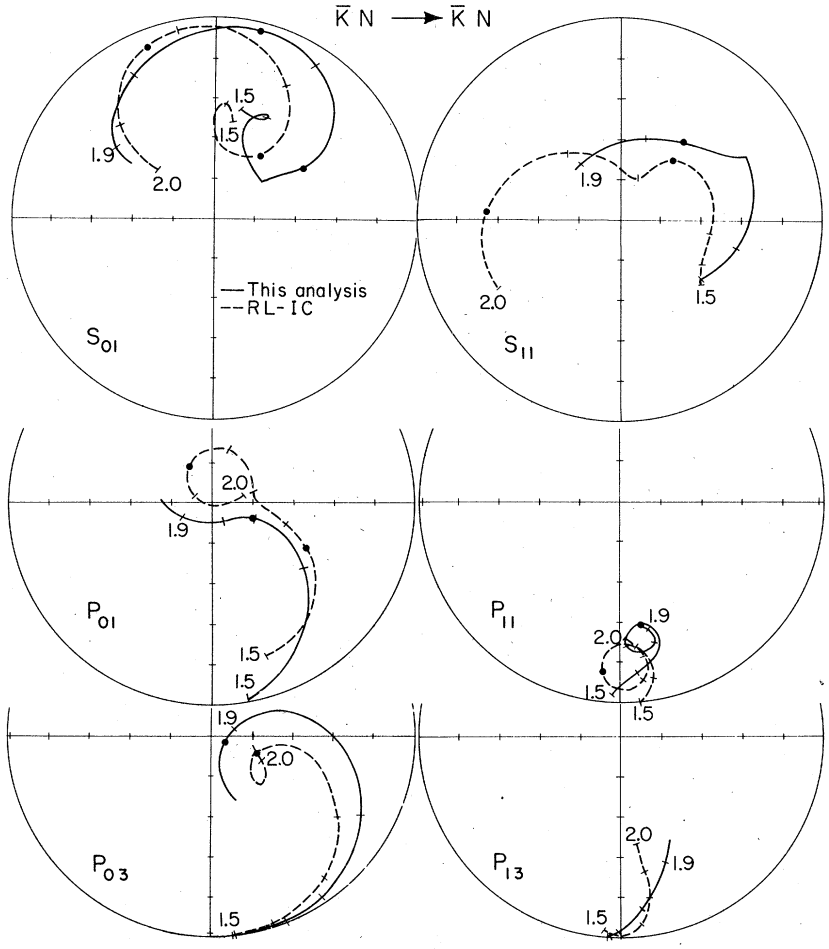

FIG. 1. Argand diagrams of the S- and P-wave amplitudes. The solid curves are the results of this analysis while the dashed curves show the RL-IC (Ref. 8) solution. Numbers are c.m. energies in GeV with intervals of 0.1 GeV indicated by bars. The locations of resonance masses in each partial wave are indicated by circles. S-wave cups at $\Lambda\eta$ and $\Sigma^0\eta$ thresholds are explicitly accomodated in our analysis and manifest themselves on the Argand diagrams as singularities in speed accompanied by 90° discontinuities in direction (Ref. 33).

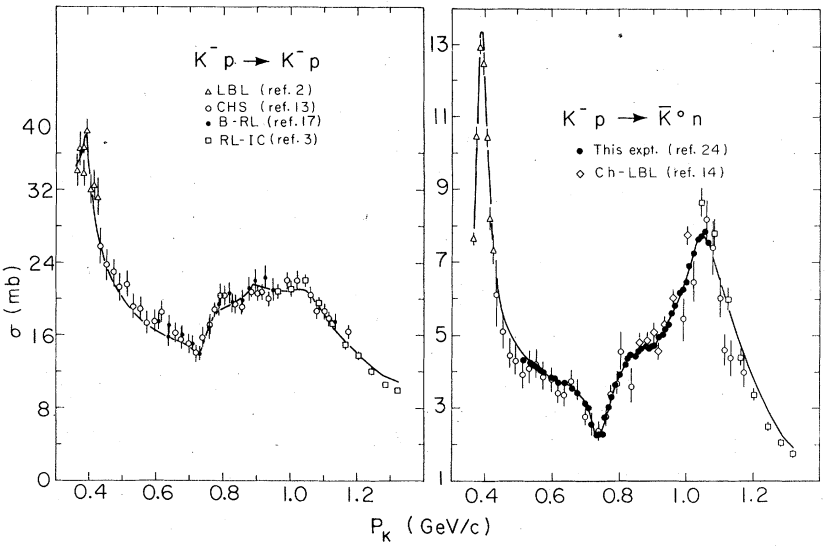

FIG. 2. The total elastic and charge-exchange cross sections calculated in this analysis and compared to the experimental data which we fit.

in Fig. 8. Figure 9 shows the measured charge-exchange differential cross section at 0° and 180° compared with our fit. We also compare the 0° cross section with the dispersion-relation prediction of Ref. 12. Predictions for the so-far-unmeasured charge-exchange polarization and for the K^-n angular distribution and polarization are shown at selected momenta along with those of other analyses in Fig. 10.

A. *S* waves

We first discuss the individual partial-wave amplitudes shown in Fig. 1 with emphasis on their resonant structure. Both the S_{01} and S_{11} amplitudes exhibit cusp behavior at their respective $\Lambda\eta$ and $\Sigma\eta$ threholds. The need for cusps is most evident in our precision measurement of the charge-exchange cross section.[24] Here the rapid variations observed in this cross section as the thresholds are traversed cannot be followed with the cusps suppressed. Figure 11 is an expanded view of the region of these thresholds showing the fits to our data with and without cusps along with a comparison of χ^2 for the two cases.

In addition to the narrow S_{01} resonance at $\Lambda\eta$ threshold,[31] we find that a second broad resonance in this amplitude makes a substantial improve-

TABLE III. Background and cusp parameters as defined in Eqs. (3), (2), and (5).

Amplitude	a_1	b_1	a_2	b_2	a_3	b_3
S_{01}	−0.536	1.401	−0.001	−0.807	0.145	0.280
S_{11}	0.287	0.783	0.045	0.019	0.217	0.084
P_{01}	0.078	0.746	−0.487	0.079	−0.497	−0.147
P_{11}	0.085	0.416	0.105	0.022	−0.108	0.012
P_{03}	0.387	0.155	0.150	0.280	0.091	0.045
P_{13}	0.030	0.159	0.175	0.356		
D_{03}	0.227	−0.332				
D_{13}	0.130	−0.384				
D_{05}	0.125					
D_{15}	0.037					
F_{05}	−0.033					
F_{15}	0.000					
F_{07}	0.039					
F_{17}	0.025					
G_{07}	0.059					
G_{17}	0.030					
		R	2.20 F			
		γ_Λ	0.104			
		γ_Σ	0.385			

TABLE IV. Partial-wave amplitudes $\times 10^3$. These are listed every 20 MeV/c with the real part above the imaginary part.

P_{beam} (GeV/c)	$E_{c.m.}$ (GeV)	S_{01}	S_{11}	P_{01}	P_{11}	P_{03}	P_{13}	D_{03}	D_{13}	D_{05}	D_{15}	F_{05}	F_{15}	F_{07}	F_{17}	G_{07}	G_{17}
0.360	1.5069	66	207	111	−16	61	−36	176	6	4	7	1	0	0	1	0	0
		773	346	28	26	5	8	81	5	0	0	0	0	0	0	0	0
0.380	1.5144	71	207	132	−15	69	−39	222	8	5	8	2	0	0	1	0	0
		770	349	44	29	6	9	294	6	0	0	0	0	0	0	0	0
0.400	1.5221	77	207	154	−13	76	−41	−122	10	6	10	2	1	0	1	1	0
		767	352	63	32	7	9	410	7	0	0	0	0	0	0	0	0
0.420	1.5299	82	206	174	−11	84	−43	−210	12	8	12	3	1	1	1	1	0
		763	353	86	35	8	8	204	9	0	0	0	0	0	0	0	0
0.440	1.5379	88	206	193	−8	92	−45	−179	14	9	15	4	1	1	2	1	0
		760	355	112	39	10	8	120	10	0	0	0	0	0	0	0	0
0.460	1.5461	94	205	209	−5	100	−46	−151	16	10	18	4	1	1	2	1	0
		757	356	142	42	11	8	85	12	0	1	0	0	0	0	0	0
0.480	1.5545	100	205	222	−1	108	−47	−130	19	12	21	6	1	1	2	2	0
		755	356	173	46	13	7	69	14	0	1	0	0	0	0	0	0
0.500	1.5630	106	205	231	4	117	−48	−113	22	13	25	7	2	1	3	2	0
		752	356	206	49	15	7	60	16	0	1	0	0	0	0	0	0
0.520	1.5716	111	204	235	9	125	−48	−100	26	15	29	8	2	2	3	2	0
		751	357	239	53	17	6	54	18	0	2	0	0	0	0	0	0
0.540	1.5803	117	205	236	15	134	−48	−87	30	17	33	10	3	2	4	3	0
		750	357	272	57	19	6	52	21	0	3	0	0	0	0	0	0
0.560	1.5891	122	205	232	21	143	−48	−76	34	19	38	12	3	2	5	4	1
		750	357	302	61	22	5	50	24	0	3	0	0	0	0	0	0
0.580	1.5980	126	206	226	28	153	−47	−64	39	21	44	15	4	2	5	4	1
		751	357	331	66	25	5	50	27	0	4	0	0	0	0	0	0
0.600	1.6070	129	208	216	35	162	−46	−51	45	23	50	18	4	3	6	5	1
		753	358	356	71	29	5	51	32	1	6	1	0	0	0	0	0
0.620	1.6160	130	210	206	44	172	−44	−38	52	25	57	21	5	3	7	6	1
		756	358	378	76	33	4	54	37	1	8	1	0	0	0	0	0
0.640	1.6251	128	213	194	53	182	−42	−23	59	27	65	24	6	3	8	7	1
		759	360	397	83	37	4	59	44	1	10	1	0	0	0	0	0
0.660	1.6343	120	217	181	63	193	−40	−6	68	29	74	29	6	4	9	8	1
		761	362	413	91	42	4	66	54	1	13	1	0	0	0	0	0
0.680	1.6435	105	222	169	74	203	−37	13	76	31	83	33	7	4	10	10	1
		757	364	426	102	48	5	79	68	1	17	2	0	0	0	0	0
0.700	1.6528	81	229	156	85	214	−34	34	82	34	94	39	8	5	11	11	2
		733	368	437	119	54	5	100	89	1	22	3	1	0	0	0	0
0.720	1.6621	80	237	144	92	225	−30	52	78	36	106	45	9	5	13	12	2
		644	374	446	146	61	6	132	118	2	29	4	1	0	1	0	0
0.740	1.6714	230	246	133	78	236	−26	57	56	38	119	53	11	5	14	14	2
		632	381	452	180	68	8	180	144	2	38	5	1	0	1	0	0
0.760	1.6807	293	258	123	37	247	−22	35	22	41	133	61	12	6	15	16	2
		728	392	457	191	77	9	233	152	2	49	7	1	0	1	1	0
0.780	1.6901	286	271	113	13	259	−17	−16	−4	43	148	71	13	6	17	18	2
		818	405	461	167	87	11	268	139	2	64	9	1	0	1	1	0
0.800	1.6995	250	285	104	15	270	−12	−73	−15	46	163	82	15	7	19	20	3
		882	424	463	144	97	14	267	121	3	84	12	2	0	1	1	0
0.820	1.7089	203	301	95	25	282	−7	−112	−16	49	177	95	17	7	20	22	3
		927	449	465	132	109	17	242	107	3	110	16	2	0	1	1	0
0.840	1.7183	150	316	87	35	293	−2	−130	−13	51	189	111	18	8	22	24	3
		957	484	466	127	122	20	212	97	4	142	22	3	0	2	1	0
0.860	1.7277	95	328	80	45	305	4	−135	−9	54	194	129	20	8	24	27	3
		973	531	466	126	136	24	187	90	4	183	31	3	0	2	2	0
0.880	1.7372	41	328	73	53	316	10	−133	−4	57	189	150	23	9	26	29	4
		978	600	466	127	152	28	167	87	5	230	42	4	0	2	2	0
0.900	1.7466	−10	262	66	60	327	16	−129	1	59	169	175	25	9	29	32	4
		973	661	465	129	170	33	153	84	6	280	59	5	0	3	2	0
0.920	1.7560	−57	217	59	66	337	22	−123	5	62	131	204	27	10	31	35	4
		960	678	464	132	189	39	141	83	7	326	83	6	0	3	3	0

TABLE IV. (*Continued*)

P_{beam} (GeV/c)	$E_{c.m.}$ (GeV)	S_{01}	S_{11}	P_{01}	P_{11}	P_{03}	P_{13}	D_{03}	D_{13}	D_{05}	D_{15}	F_{05}	F_{15}	F_{07}	F_{17}	G_{07}	G_{17}
0.940	1.7654	−98	178	53	71	346	28	−116	9	65	77	236	30	10	33	38	5
		941	690	462	134	210	45	133	83	9	358	120	7	0	4	4	0
0.960	1.7748	−133	143	46	75	354	35	−109	13	68	17	268	33	11	36	42	5
		919	698	461	138	232	52	127	83	11	371	173	9	0	5	4	0
0.980	1.7842	−162	110	39	79	361	41	−103	17	70	−41	291	36	11	39	45	5
		895	702	459	141	257	59	122	84	13	363	251	11	0	6	5	0
1.000	1.7936	−186	81	32	82	366	47	−97	20	71	−88	289	40	12	42	49	5
		870	703	457	144	285	67	118	85	15	341	357	13	0	7	6	0
1.020	1.8030	−205	54	25	84	368	53	−91	23	72	−123	235	44	13	45	53	6
		845	702	456	148	314	75	115	86	18	312	478	16	0	8	7	0
1.040	1.8123	−220	30	18	86	368	59	−85	26	71	−146	115	47	13	48	57	6
		822	698	454	151	346	84	113	88	20	280	573	19	0	9	8	0
1.060	1.8217	−231	9	10	87	363	65	−79	29	70	−160	−39	51	14	52	62	6
		799	694	453	154	379	93	111	89	21	250	597	24	0	11	10	0
1.080	1.8310	−240	−10	1	88	354	71	−74	31	69	−168	−170	55	14	56	66	7
		778	688	452	157	415	103	110	91	21	223	549	29	0	13	11	0
1.100	1.8403	−245	−27	−8	88	338	77	−69	34	68	−171	−251	59	15	60	71	7
		758	682	451	160	452	113	109	92	20	200	469	35	0	15	13	0
1.120	1.8496	−249	−41	−17	87	314	82	−64	36	69	−171	−290	63	15	64	76	7
		740	676	451	164	487	124	108	94	18	179	390	43	0	17	15	0
1.140	1.8589	−250	−54	−27	86	280	88	−59	39	70	−169	−304	66	16	68	82	8
		723	669	451	167	520	135	107	96	16	162	324	52	0	20	18	0
1.160	1.8681	−250	−65	−38	85	237	93	−54	41	72	−166	−304	67	16	73	87	8
		708	663	453	170	546	147	107	98	15	147	272	63	0	24	21	0
1.180	1.8774	−248	−74	−49	83	186	97	−50	43	74	−163	−297	67	17	78	93	8
		695	657	455	172	559	159	107	99	14	134	232	74	0	28	24	0
1.200	1.8866	−245	−82	−60	80	132	102	−45	45	76	−159	−289	65	18	83	99	9
		683	650	459	175	557	171	107	101	13	123	201	87	0	32	28	0
1.220	1.8958	−241	−89	−71	77	81	106	−41	47	78	−154	−279	59	18	88	106	9
		672	645	464	178	536	183	107	103	12	114	176	100	0	38	33	0
1.240	1.9049	−235	−94	−82	73	43	110	−37	49	81	−150	−270	50	19	93	112	9
		662	639	470	181	498	196	107	105	12	105	157	113	0	44	38	0
1.260	1.9141	−228	−99	−93	69	24	113	−33	51	83	−146	−261	38	19	97	119	10
		654	634	478	183	452	209	107	107	12	98	141	123	0	52	43	0
1.280	1.9232	−221	−103	−104	64	23	117	−29	52	85	−142	−253	24	20	102	126	10
		648	629	487	186	406	222	108	108	12	91	129	131	0	61	50	0
1.300	1.9323	−212	−106	−113	59	39	120	−25	54	87	−138	−245	9	20	106	132	11
		642	625	498	189	368	235	108	110	12	86	118	135	0	71	57	0
1.320	1.9413	−202	−108	−122	53	64	122	−21	56	89	−135	−238	−7	21	109	139	11
		638	621	510	191	342	249	109	112	12	81	109	135	0	83	66	0
1.340	1.9504	−192	−110	−129	47	93	125	−17	57	91	−131	−232	−21	21	111	146	11
		635	618	522	194	327	262	109	114	12	76	102	132	0	96	76	0

ment in χ^2. This resonance overlaps the lower one so that the manner in which the two resonances are combined with each other as well as with the large S_{01} background seems to influence the mass found for the upper resonance. Thus, although our Argand diagram is similar to that of the RL-IC analysis,[8] the mass they obtain for the upper resonance is about 100 MeV higher than ours. On the other hand, the two analyses for the lower-mass narrow resonance are in reasonable accord with each other and with evidence found for the resonance in the $\Lambda\eta$ channel. A comparison is made in Table V of the parameters deduced for this and other S- and P-wave resonances found both by our single-channel analysis and by others.[8,31,32,35-38]

The mass and width of the S_{11} resonance near $\Sigma\eta$ threshold agree fairly well with the values found from $\Sigma\eta$ production[32] and with those found by the RL-IC analysis.[8] A second S_{11} resonance has also been suggested by RL-IC to lie just above our region of investigation. We do not confirm this resonance because the introduction of this additional structure into our program did not bring about an improvement in χ^2.

B. *P* waves

The presence of a substantial and rapidly growing P-wave amplitude in our lower momentum region

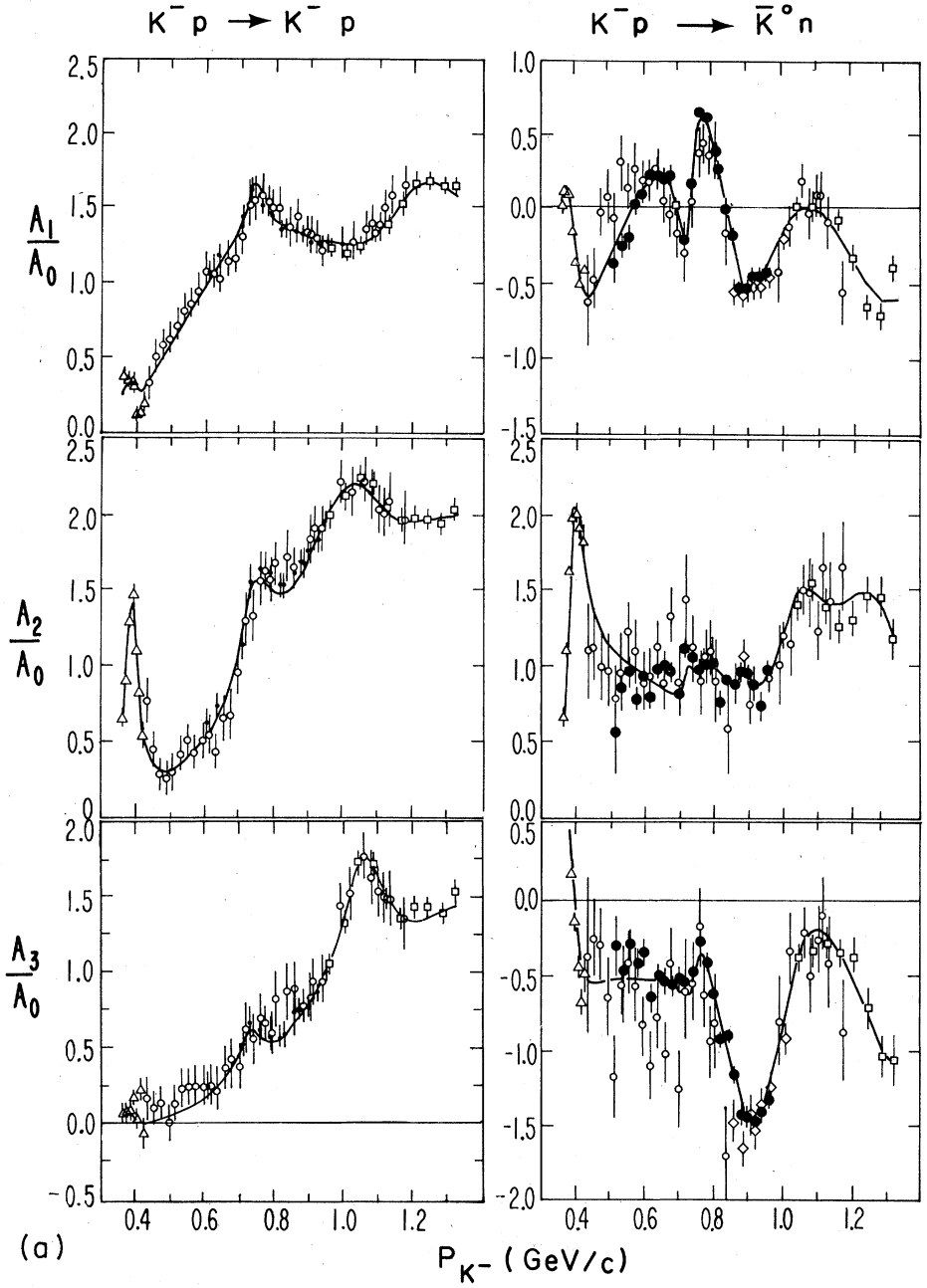

FIG. 3. The Legendre-polynomial-coefficient ratios A_n/A_0 of the angular distributions for elastic and charge-exchange scattering calculated in this analysis and compared to the experimental coefficients which we fit. Symbols are as in Fig. 2 except for "This expt." which refers to Ref. 11.

is most evident in the swift rise in the A_1/A_0 coefficient for K^-p elastic scattering as seen in Fig. 3. This leads to a very low value of the 180° elastic cross section in the vicinity of 600 MeV/c (Fig. 4). Neither of these behaviors is well-fitted either by our analysis or by others. Most agree that the P-wave interference needed to produce this behavior comes mainly from the P_{01} amplitude, and there have been several suggestions that it resonates in the vicinity of 1600 MeV.[5,8] With the addition of our new charge-exchange angular distributions, the mass and width of this resonance have changed considerably from that of our previous analysis,[9] which did not contain

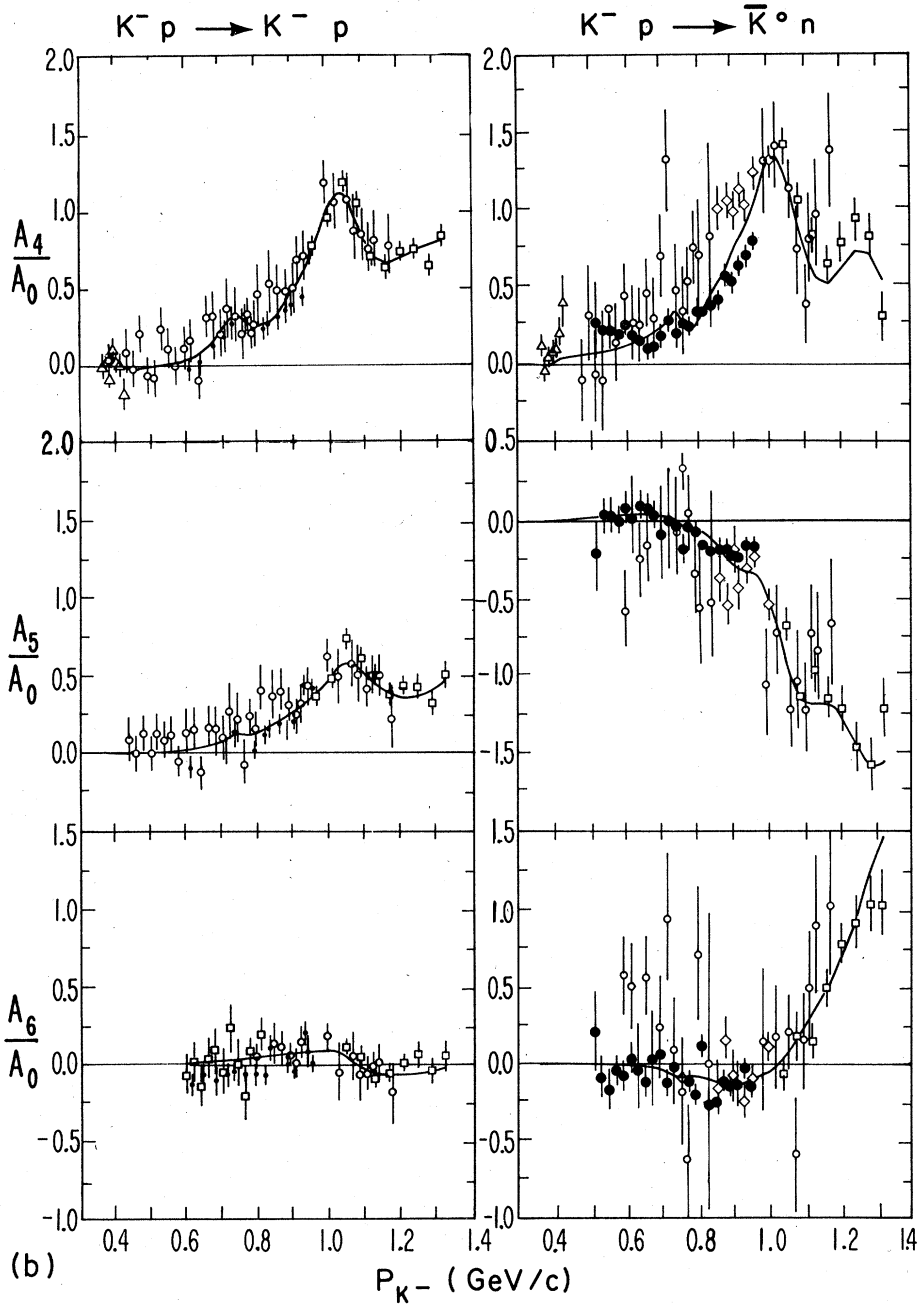

FIG. 3. *(continued)*

these data. We now obtain a mass of 1700 MeV and a very broad width of about 600 MeV. There has been a recent theoretical suggestion[39] for the inclusion of a ninth member into the stable $J^p = \frac{1}{2}^+$ baryon octet with this mass, with an elasticity of 0.23, and with an even greater width of approximately 1000 MeV. Given the large uncertainty associated with such a broad resonance, our solution is compatible with this interpretation. However, a different parametrization of the background can seriously alter the values found for such a broad resonance without appreciably affecting the Argand diagram. Thus although the mass and width found in this analysis are quite different from those found in the RL-IC analysis and even from our previous work, the Argand

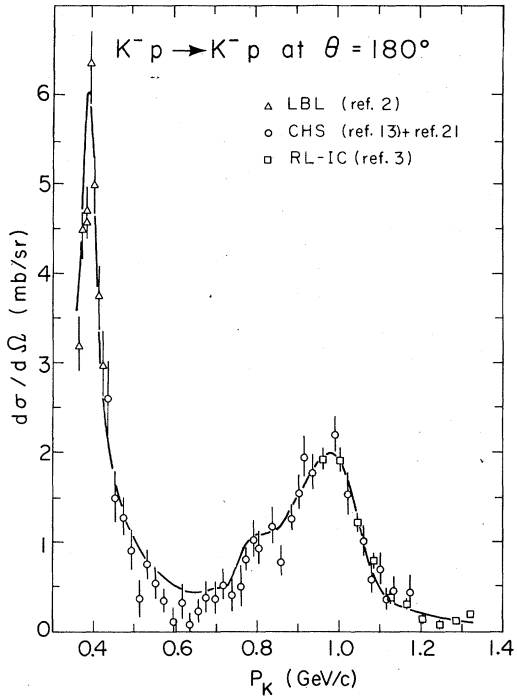

FIG. 4. The differential cross sections at 180° for elastic K^-p scattering calculated in this analysis and compared to the experimental data which we fit.

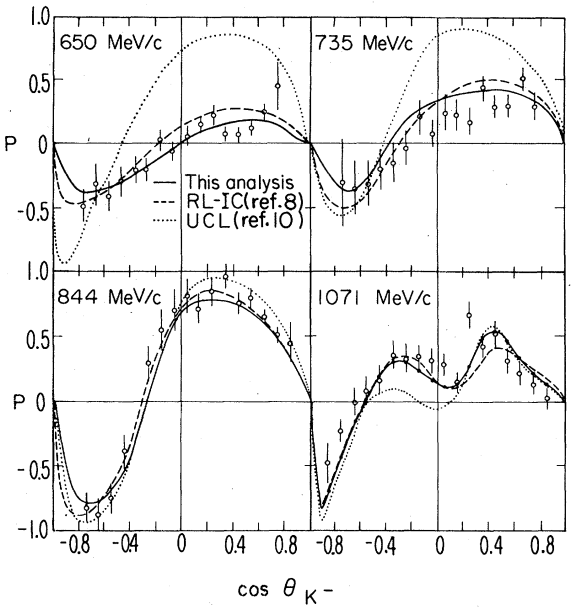

FIG. 5. Fits to some of the recently measured polarizations of Ehrlich *et al.* (Ref. 23) in K^-p elastic scattering at selected momenta.

diagrams are very similar.

A second P_{01} resonance at a higher mass has been suggested by the RL-IC analysis, but when introduced into our program was not found to yield a lower χ^2.

The recent improvements in the data bank in the $\bar{K}N$ channel have led to much better evidence for a relatively narrow resonance in the P_{11} amplitude in the intricate region between 700 and 800 MeV/c, where three other amplitudes are known to resonate. Our P_{11} resonance parameters agree quite well with those of Hart,[35] who relies heavily on unpublished higher-statistics $\bar{K}N$ bubble-chamber data in this region. However, we are only in vague accord with the RL-IC analysis, which finds very different values for this resonance in their $\bar{K}N$ and in their $\Sigma\pi$ analyses (see Table V), leading them to suggest that there are in fact two distinct resonances. Since our $\bar{K}N$ and their $\Sigma\pi$ analysis agree in mass, this now appears to be an unnecessary complication. This resonance is nearly degenerate in mass and width with the well-established $D_{13}(1670)$.

The P_{03} amplitude grows to prominence throughout our energy region, but, as with other analyses, we find that this large amplitude is better parametrized at lower energies as a background with a clear resonance appearing only near 1900

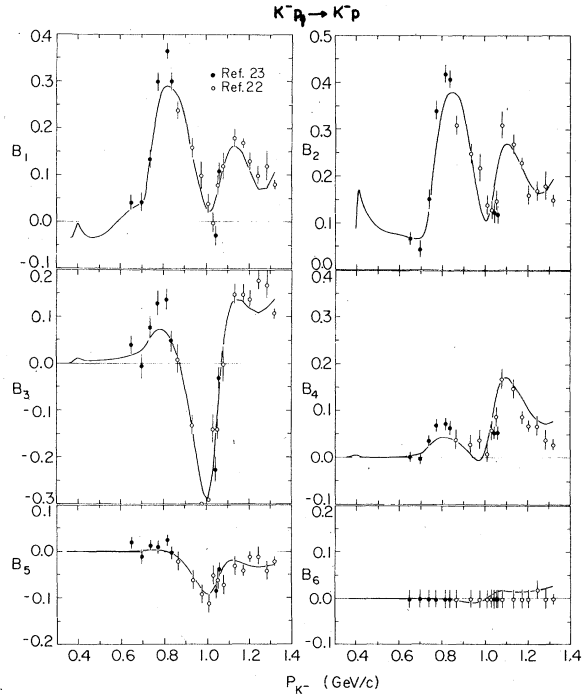

FIG. 6. The experimental polynomial coefficients B_n of the product $I\!P = \bar{\lambda}^2 \Sigma B_n P_n^1$ of the K^-p angular distribution times the polarization plotted at the momenta where we fitted the polarization directly and compared to the predictions of our partial-wave analysis.

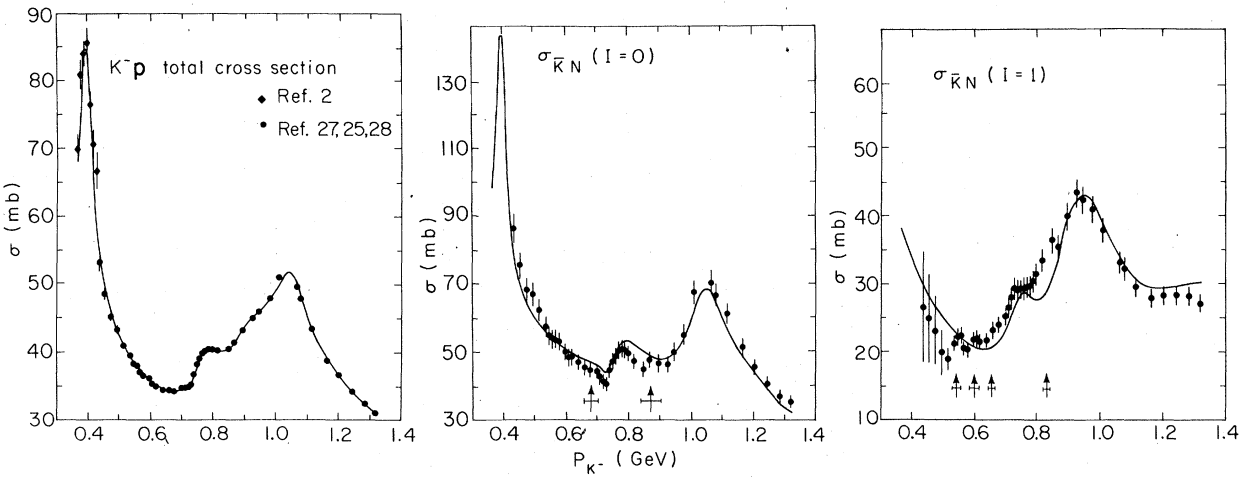

FIG. 7. The total K^-p cross sections and the $I=0$ and $I=1$ cross sections used in this analysis compared with our fit. The arrows indicate the locations and widths of six new resonances claimed by Carroll *et al* (Ref. 27).

TABLE V. *S*- and *P*-wave resonance parameters. Comparison of this work with some other single-channel analyses.

Resonance	Analysis	Channel	Mass (MeV)	Width (MeV)	Amplitude[a]
S_{01}(I)	Berley *et al.* (Ref. 31)	$\Lambda\eta$	1666	22	0.24
	CHS (Ref. 36)	$\bar{K}N$	1663	26	0.14
	RL-IC (Ref. 8)	$\bar{K}N$	1670	45	0.17
	RL-IC (Ref. 8)	$\Sigma\pi$	1670	45	0.35
	This analysis	$\bar{K}N$	1671	29	0.17
S_{01}(II)	Bricman *et al.* (Ref. 37)	$\bar{K}N$	1872	100	0.18
	RL-IC (Ref. 8)	$\bar{K}N$	1823	230	0.39
	This analysis	$\bar{K}N$	1725	185	0.28
S_{11}(I)	Jones (Ref. 32)	$\Sigma\eta$	1760	92	0.23
	RL-IC (Ref. 8)	$\bar{K}N$	1768	60	0.14
	RL-IC (Ref. 8)	$\Lambda\pi$	1710	68	0.09
	This analysis	$\bar{K}N$	1770	161	0.33
S_{11}(II)	RL-IC (Ref. 8)	$\bar{K}N$	1955	200	0.49
P_{01}(I)	RL-IC (Ref. 8)	$\bar{K}N$	1567	117	0.24
	RL-IC (Ref. 8)	$\Sigma\pi$	1584	191	0.17
	This analysis	$\bar{K}N$	1703	593	0.14
P_{01}(II)	RL-IC (Ref. 8)	$\bar{K}N$	1856	144	0.22
	RL-IC (Ref. 8)	$\Sigma\pi$	1846	180	0.20
P_{11}	Hart (Ref. 35)	$\bar{K}N$	1658	40	0.11
	RL-IC (Ref. 8)	$\bar{K}N$	1738	72	0.14
	RL-IC (Ref. 8)	$\Sigma\pi$	1676	117	0.16
	This analysis	$\bar{K}N$	1679	38	0.10
P_{03}	Conforto *et al.* (Ref. 38)	$\bar{K}N$	1883	80	0.25
	RL-IC (Ref. 8)	$\bar{K}N$	1900	72	0.18
	This analysis	$\bar{K}N$	1908	119	0.34

[a] In our analysis the amplitude shown for the elastic channel when significant absorptive backgrounds are present is $\eta_B\Gamma_e/\Gamma$, corresponding to the diameter of the resonant circle. The amplitudes for other reactions, $(\Gamma_e\Gamma_i)^{1/2}/\Gamma$ are listed here only to indicate the strength of the signal in that channel.

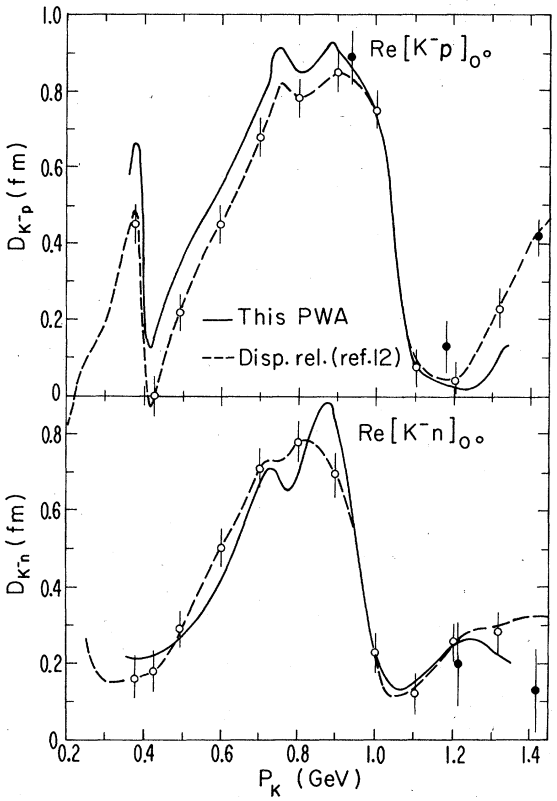

FIG. 8. The real parts of the K^-p and K^-n forward scattering amplitudes in the laboratory frame calculated by this analysis and compared to a dispersion-relation calculation. The latter were introduced into the fit at approximately 100 MeV/c intervals with errors of ± 0.05 fm as indicated by the open circles. Solid points correspond to actual measurements of real parts.

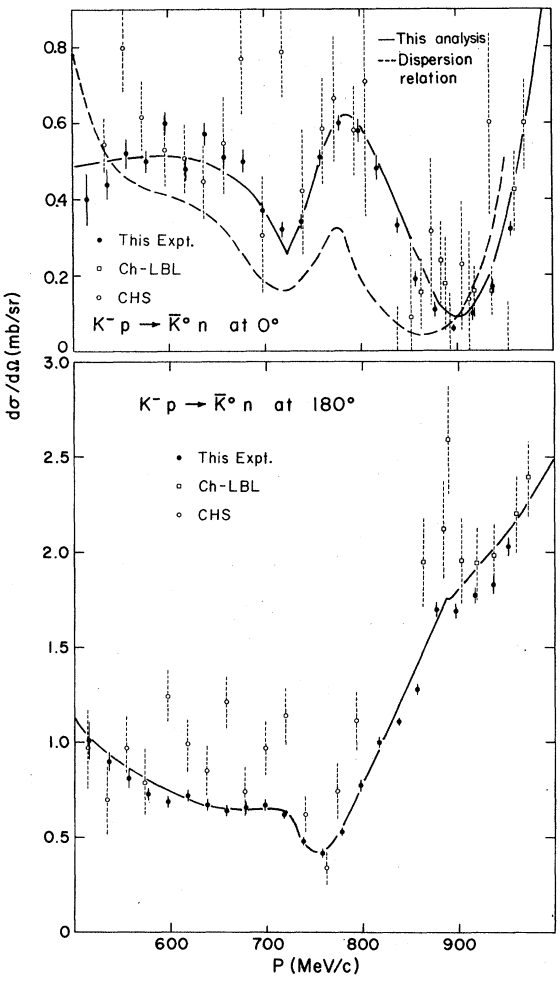

FIG. 9. The measured charge-exchange differential cross sections at 0° and 180° compared with the fit of this partial-wave analysis. The 0° cross section predicted from the dispersion relation of Martin (Ref. 12) is also shown.

MeV. Apart from the well-known Σ (1385), the P_{13} amplitude shows no resonant behavior, in agreement with other studies.

C. Other waves

Most partial-wave analyses agree concerning the existence and parameters of resonances in higher-angular-momentum states. In our former analysis,[9] the $D_{13}(1670)$, which is known to have a relatively weak coupling to the $\bar{K}N$ channel, gave a mass and width discordant with better evidence from other channels. However, with the addition of our angular distribution data, these parameters are now in excellent agreement with accepted values.

Finally we consider the recent indications for a number of narrow $\bar{K}N$ states found by Carroll *et al.*,[27] in the analysis of their total K^-p and K^-d cross sections. Although neither of these measured cross sections shows direct evidence for new structure, when decomposed into pure isospin cross sections, four new resonances emerge in the $I=1$ channel and two in $I=0$, all lying between 500 and 900 MeV/c. They appear as narrow structures with low elasticity, and their locations are indicated by arrows in Fig. 7. None of the other data in the $\bar{K}N$ channel show any evidence for these structures, although most are too poor in statistical accuracy to reveal resonances so weakly coupled to the elastic channel. However, support for the most prominent of these structures, the $I=1$ bump at 546 MeV/c (1582 MeV) comes from reanalysis of CHS bubble-chamber data by Litchfield,[40] who identifies a D_{13} resonance of nearly identical mass and width in the reaction

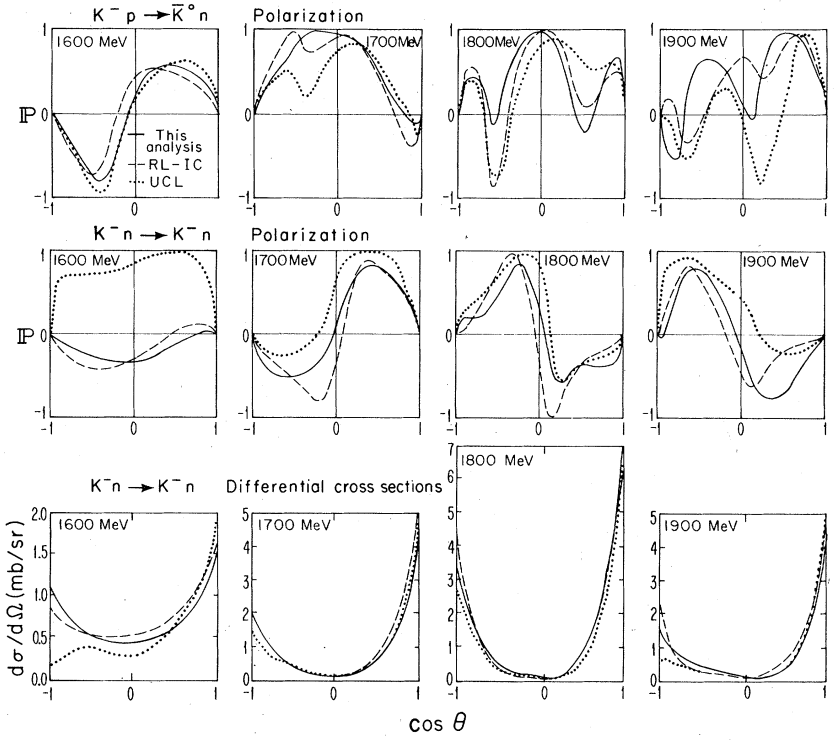

FIG. 10. Comparison between our predictions (solid lines), those of the RL-IC analysis (dashed lines) and those of UCL (dotted lines) for the unmeasured charge-exchange polarization and for the K^-n polarization and angular distribution at selected c.m. energies as a function of the K^- c.m. scattering angle.

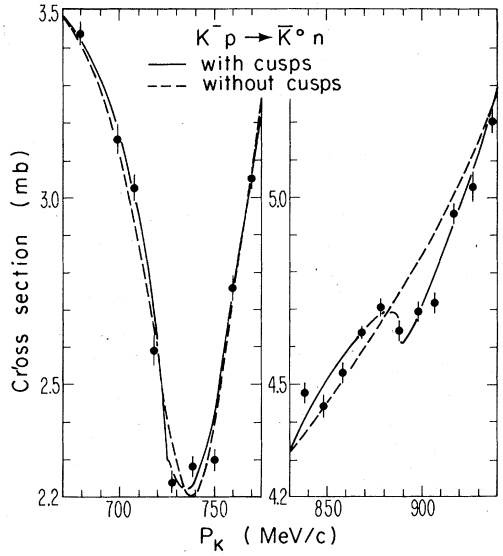

FIG. 11. Expanded view of the fit to our precision charge-exchange cross sections of Ref. 24 in the vicinity of $\Lambda\eta$ and $\Sigma^\circ\eta$ thresholds showing the best overall fit obtained with and without cusps. The χ^2 coming from these 20 data points in ±50-MeV/c intervals surrounding the thresholds is 55 with cusps and 185 without cusps. The total χ^2 decreases by 266 when the additional two degrees of freedom associated with the two cusp parameters γ_Λ and γ_Σ are introduced.

$K^-p \to \Lambda\pi$. In our previous work[9] we investigated the consistency of $I=1$ resonances at 546 and 602 MeV/c with the rest of the $\bar{K}N$ data and concluded that if they exist they are probably not in the S or P states. Our charge-exchange angular-distribution experiment showed no evidence for new structures, and one must await further precise measurements to resolve these questions.

D. Discussion of results

In Table II we have indicated by stars the status of hyperon resonances in 1976 as assigned by the Particle Data Group,[34] and in parentheses have shown the changes in this attribution which we believe should be made on the basis of this analysis.

We next consider the uncertainties inherent in this particle-wave analysis. The problems of ambiguities that have troubled the energy-independent pion-nucleon partial-wave analyses have been of less concern in the $\bar{K}N$ system where, because the data are generally not as precise, energy-dependent analyses have been the rule. Here with several prominent Y^* resonances [such as the $D_{03}(1520)$, $D_{15}(1765)$, and $F_{05}(1815)$, whose quantum numbers have been established

by a variety of means] extending over most of the fitted interval, ambiguities are effectively removed. Only in the mass region of 1600 MeV, where there are no prominent structures, could there be any possibility of radically different solutions fitting the data equally well.

A more legitimate concern centers on the manner in which the background is parametrized and how this affects the parameters and even the need for the less prominent resonances. In this regard it is illuminating to compare our analysis with the recent RL-IC work,[8] where the backgrounds were introduced in a very different way. A comparison of the Argand diagrams of the lower partial waves for the two analyses can be found in Fig. 1. The general structures appear very similar and will probably remain as lasting features of future partial-wave analyses. It is in the interpretation of these features in terms of resonances, particularly when they are broad and of low elasticity, where the somewhat arbitrary choice of background complexity and parametrization plays an important role. The differences in resonance parameters found by the two analyses reflect this uncertainty.

We have also explored another expansion for the background. As an alternative to the chosen parametrization [Eq. (3)], the a and b coefficients of the scattering length $A = a + ib^2$ were instead expanded as

$$a = \sum_n a_n \left(\frac{P}{E}\right)^{2n} \text{ and } b = \sum_n b_n \left(\frac{P}{E}\right)^{2n}, \qquad (6)$$

where P and E are the c.m. momentum and energy. For low energies such a dependence would be suggested by the effective-range expansion. This yielded $\chi^2 = 2842$, i.e., more than 300 higher than our best fit. Since this new parametrization is less adaptable to variations at low energy, it may argue for the existence of further structure in the lower part of our energy region, where the data indicate that there are deficiencies in the parametrization. Unfortunately it is here, in the region above 400 and below 700 MeV/c, that the measurements are least accurate.

We have also tried to reduce the number of background parameters since an over-parametrized background can to some degree simulate a resonance or at least reduce its contribution. On the basis of these attempts, a case could be made for diminishing the number of parameters for the P_{11}, P_{03}, and P_{13} backgrounds, while the other amplitudes appear to require the chosen expansion. It should be noted that the background amplitudes alone tend to have counterclockwise Argand trajectories as a function of energy in the manner of resonances, although with a different energy dependence. With these considerations in mind, it is likely that a more refined analysis with better data will reveal greater resonant contributions to the amplitudes and perhaps more broad resonances than the solution which we present here.

The uncertainties we assign to the resonance parameters appearing in Table II were estimated by studying the change when the backgrounds were altered in various ways described above, as well as by investigating the stability of the parameters to the removal of our charge-exchange angular-distribution data. There is, of course, further information available about many of these resonances from other two-body channels, particularly if the resonance in question has a large branching fraction into another channel.

Finally we consider how this analysis and those of RL-IC (Ref. 8) and UCL (Ref. 10) differ with regard to directly measurable quantities. In Fig. 5 we exhibit the polarization in K^-p elastic scattering at several recently measured momenta. Both our analysis (which uses these data), and that of RL-IC lead to very nearly the same polarization, in good agreement with experiment. However the UCL amplitudes do not accommodate the rapidly diminishing polarization displayed by the data below 750 MeV/c. Since their $J = \frac{1}{2}$ amplitudes, in both S and P waves, differ substantially from ours and from RL-IC at low momenta, the K^-p polarization reflects this difference. Presumably the major reason for this difference lies in the fact that UCL did not use the high-statistics bubble-chamber data in the vicinity of 400 MeV/c to stabilize the amplitudes at low momentum. In Fig. 10 the predictions for the unmeasured $\bar{K}^0 n$ and K^-n polarizations and the K^-n differential cross sections are displayed at four c.m. energies. Again there are generally only minor differences between our solution and that of RL-IC, whereas a major difference in K^-n polarization at low energy distinguishes the UCL solution from the others.

V. CONCLUSIONS

We have presented in Table II our best estimates of the status and parameters of hyperon resonances with masses between 1500 and 1950 MeV. These are based on our partial-wave analysis of all the latest available $\bar{K}N$ data from formation experiments. Our amplitudes are in good agreement with those of similar analysis of older data by the RL-IC group,[8] although certain resonance parameters differ significantly. Some of these differences probably result from the inclusion of new precision data while others, pertaining

to the broad resonances, can be ascribed to different background parametrizations and to a different way of combining resonances and backgrounds. On the other hand, our amplitudes in low partial waves disagree substantially with the recent UCL solution[10] at low momentum where new polarization measurements have shown the UCL solution to be in error.

Most of the momentum-dependent structure within the $\bar{K}N$ data bank can be well-fitted by the contemporary set of resonances with no compelling necessity for the introduction of further resonances. However, data between 430 and 700 MeV/c are sparse, sometimes discordant, and occasionally difficult to fit. Since there are no prominent resonances in this region to guide the analysis, additional experimental work here would be highly desirable. In particular, it would be of interest to redetermine the individual $I=1$ and $I=0$ total cross sections to ascertain the systematic uncertainty inherent in the currently available cross sections and the reliability of the structures claimed therein.

ACKNOWLEDGMENT

This work was supported in part by the U.S. Department of Energy.

[1]W. E. Humphrey and R. R. Ross, Phys. Rev. 127, 1305 (1962); M. B. Watson, M. Ferro-Luzzi, and R. D. Tripp, *ibid.* 131, 2248 (1963); J. K. Kim, Phys. Rev. Lett. 14, 29 (1965).
[2]LBL: T. S. Mast *et al.*, Phys. Rev. D 14, 13 (1976).
[3]RL-IC: B. Conforto *et al.*, Nucl. Phys. B105, 189 (1976).
[4]CHS: R. Armenteros *et al.*, Nucl. Phys. B3, 592 (1967); B8, 195 (1968); B14, 91 (1969).
[5]J. K. Kim, Phys. Rev. Lett. 27, 356 (1971).
[6]W. Langbein and F. Wagner, Nucl. Phys. B47, 477 (1972).
[7]A. T. Lea *et al.*, Nucl. Phys. B56, 77 (1973).
[8]RL-IC: G. P. Gopal *et al.*, Nucl. Phys. B119, 362 (1977).
[9]M. Alston-Garnjost *et al.*, Phys. Rev. Lett. 38, 1007 (1977).
[10]UCL: B. R. Martin and M. K. Pidcock, Nucl. Phys. B126, 285 (1977).
[11]M. Alston-Garnjost *et al.*, Phys. Rev. D 17, 2226 (1978).
[12]A. D. Martin, Phys. Lett. 65B, 346 (1976); and private communication.
[13]CHS: R. Armenteros *et al.*, Nucl. Phys. B8, 233 (1968); B21, 15 (1970).
[14]M. Jones *et al.*, Nucl. Phys. B90, 349 (1975).
[15]A. Bigi *et al.*, Nucl. Phys. B110, 25 (1976); Y. Cho *et al.*, Phys. Lett. 60B, 293 (1976).
[16]R. Armenteros *et al.*, Nucl. Phys. B18, 425 (1970); N. N. Jew and G. E. Kalmus, *ibid.* B22, 205 (1960).
[17]G. J. Adams *et al.*, Nucl. Phys. B96, 54 (1975).
[18]P. Baillon *et al.*, Nucl. Phys. B105, 365 (1976); B107, 189 (1976); P. Jenni *et al.*, *ibid.* B105, 1 (1976).
[19]P. Baillon *et al.*, Phys. Lett. 61B, 171 (1976).
[20]R. D. Tripp, in *Proceedings of the Topical Conference on Baryon Resonances, Oxford*, 1976, edited by R. T. Ross and D. H. Saxon (Rutherford Laboratory, Chilton, Didcot, England, 1977), p. 496.
[21]P. K. Caldwell *et al.*, Phys. Rev. D 2, 1 (1970).
[22]S. Andersson-Almehed *et al.*, Nucl. Phys. B21, 515 (1970); M. G. Albrow *et al.*, *ibid.* B29, 413 (1971).
[23]R. D. Ehrlich *et al.*, Phys. Lett. 71B, 455 (1977).
[24]M. Alston-Garnjost *et al.*, Phys. Rev. Lett. 38, 1003 (1977); Phys. Rev. D 17, 2216 (1978).
[25]D. V. Bugg *et al.*, Phys. Rev. 168, 1466 (1968).
[26]T. Bowen *et al.*, Phys. Rev. D 2, 2599 (1960).
[27]A. S. Carroll *et al.*, Phys. Rev. Lett. 37, 806 (1976).
[28]R. L. Cool *et al.*, Phys. Rev. D1, 1887 (1970).
[29]C. Michael, Phys. Lett. 21, 93 (1966).
[30]S. L. Glashow and A. H. Rosenfeld, Phys. Rev. Lett. 10, 192 (1963).
[31]D. Berley *et al.*, Phys. Rev. Lett. 15, 641 (1965).
[32]M. Jones, Nucl. Phys. B73, 141 (1974).
[33]R. H. Dalitz, *Strong Interaction Physics and Strange Particles* (Oxford Univ. Press, New York, 1962).
[34]Particle Data Group, Rev. Mod. Phys. 48, S1 (1976).
[35]E. L. Hart, in *Baryon Resonances—73*, proceedings of the Purdue Conference, edited by E. C. Fowler (Purdue Univ. Press, Lafayette, Indiana, 1973), p. 311.
[36]R. Armenteros *et al.*, Nucl. Phys. B8, 195 (1968).
[37]C. Bricman *et al.*, Phys. Lett. 33B, 511 (1970).
[38]B. Conforto *et al.*, Nucl. Phys. B34, 41 (1971).
[39]M. D. Slaughter and S. Oneda, Phys. Rev. D 14, 799 (1976).
[40]P. J. Litchfield, Phys. Lett. 51B, 509 (1974).